Loughborough University

This item was submitted to Loughborough's Institutional Repository by the author and is made available under the following Creative Commons Licence conditions.

For the full text of this licence, please go to:
http://creativecommons.org/licenses/by-nc-nd/2.5/

Threshold Fine-Tuning and 3D Characterisation of Porous Media Using X-ray Nanotomography

Hossein Ostadi, Kyle Jiang

School of Mechanical engineering, University of Birmingham, Birmingham, B15 2TT, UK

Pratap Rama, Yu Liu, Rui Chen

Department of Aeronautical and Automotive Engineering, Loughborough University, Leicestershire,
LE11 3TU, UK

Xiaoxian Zhang

Department of Engineering, University of Liverpool, Brownlow Street, L69 3GH, UK

Abstract: A common challenge in the X-ray nanotomography of porous media, such as fuel cell gas diffusion layers (GDLs), is to binarize nanotomography greyscale images in order to differentiate between solids and voids for structural characterisation and numerical flow analysis. In the process threshold determination is critical. This paper presents a study on determination of and fine-tuning threshold value based on comparison of material porosity and average fibre diameter obtained from nanotomography images with porosity data from density experiments and average fibre diameter achieved from scanning electron microscopy images respectively. The more accurate 3D reconstructed model is then used to calculate pore size distribution and average pore size, while the gas permeability of the representative 3D binary images are calculated using a single phase Lattice Boltzmann (LB) model in the D3Q19 regime.

Keywords: X-ray Nanotomography, Gas diffusion Layer (GDL), Fuel Cell, Porous material, Threshold, Lattice Boltzmann (LB).

INTRODUCTION

Nano-computed tomography (nanoCT) is a non-invasive tool for visualisation and characterization of both external and internal structures of materials with nano-scale features, such as integrated circuit (IC) chips and fuel cell gas diffusion layers (GDLs). NanoCT works by acquiring numerous views of a sample over a range of angles and creating images to map the level of X-ray attenuation in the views to the density of the sample [1]. These grey scale shadow images are then used to make 2D slices corresponding to what would be seen as the sample is cut through the scanning plane [2,3]. The slices are then assembled to reconstruct a 3D image. X-ray images can be generated using high resolution microtomography and nanotomography scanners. The former provides a resolution of 1-10 m, while the later can produce a resolution less than 100 nm [4,5].

Recently, X-ray micro and nanotomography has been used to determine the distribution of liquid water saturation in GDLs and to determine the two-phase material parameters of a GDL at resolutions of 10 μm and 700 nm respectively [6,7].

The GDL is a heterogeneous porous carbon-based material which in a fuel cell allows reactant gases to pass through to the catalyst layer [8] whilst removing any excess liquid water [9,10]. In order to accurately understand how its structural and material characteristics affect the internal flows, it requires to generate representative 3D digital models that can be used for pore analysis and numerical flow simulation tools [11]. Therefore, thresholding the greyscale shadow images from X-ray tomography is a necessary step to produce binary images which differentiate between solidity and void space [12,13]

Currently, the appropriate threshold level is often determined by visual inspection [14,15]. In one heuristic technique developed by the authors, the threshold level is determined by comparing the surface of the 3D image obtained by X-ray tomography with a reference scanning electron microscopy (SEM) image of the same surface in terms of average fibre diameter and connectivity. While the average fibre diameter is an unequivocal numerical quantity determined using software techniques, the method still relies upon visual inspection for a certain degree of tuning to ensure fibre continuity. The current method therefore invokes a delicate balance between attaining high numerical accuracy in the average fibre diameter and visual accuracy in the fibre continuity. The choice of

2

threshold fraction in this balance however has a significant effect on the volume fraction, pore size, trabecular number, morphological parameters and mechanical properties of the resulting 3D binary image [16,17]. Thus further research is needed to develop a repeatable technique by which the most suitable threshold level can be determined.

This paper proposes a method for fine-tuning the threshold of nanotomography images for porous media. Porosity and average fibre diameter of a GDL obtained from a series of thresholded Xray nanotomography images were compared to reference values of porosity and average fibre diameter achieved from density experiment and SEM images respectively. Between the thresholded images, the optimal threshold was chosen in which the porosity and average fibre diameter of the resultant digital model are most close to the reference values. The more accurate 3D tomographic images are then used to calculate morphological parameters such as pore size distribution and average pore size. The LB model [18,19] is finally applied to simulate single-phase flows through the 3D model of GDLs, in order to calculate their absolute permeabilities [20].

EXPERIMENTAL

Process examples of two GDL are introduced in this section. A carbon paper and carbon cloth GDLs were scanned using an X-ray source of 25 kV and 200 A without any filter, with 2000 ms exposure time and a rotation step of 0.5 degrees. 371 shadow images with 680 nm pixels were acquired within 40 minutes for each sample (Figs. 1a,1b). The shadow images were then processed using CTAN software to reconstruct 2D greyscale slices as shown in Fig. (1c,1d) [21].

The greyscale slices were then thresholded and assembled in order to obtain 3D binary images and for parameter calculations. A threshold was applied on the 2D greyscale image slices, which composed of up to 256 grey scales. A 5% variation in threshold (equating to 13 grey scales) was produced to analyse its effect on GDL fibre diameter and porosity.

Fibre diameter and porosity obtained from nanotomography are strongly affected by threshold variation. By varying the threshold, the fibre diameter and porosity will change. Several measurements are carried out to identify the relationship between the threshold variation and pore size. Figs. (2a, 2b) show that by increasing the threshold, the average fibre diameter fluctuates about

10% for the carbon paper and decreases about 5% for the carbon cloth while porosity increases linearly about 5% for both GDLs.

The study is focused on precisely identifying the correct threshold level in this 5% band. SEM can provide high-contrast and highresolution greyscale images of the surface of the imaged sample and therefore allows the features of the carbon fibrils of the GDL to be determined. In the current study, 4 SEM images from the corners of a 5×5 mm^2 GDL and another from the centre were taken for both samples. The average fibre diameter in each SEM image were calculated through the total area of the fibres divided by the total length of the fibres image (pixel size: 0.05 μm) using CTAN software. The average diameter was obtained to be 7.00±0.05 μm and 8.40±0.05 for carbon paper and carbon cloth respectively. Fig. (3) shows an SEM image of the sample centre.

The porosity of a material can be calculated using grammage (basis weight) and the thickness of the GDL. The solid fraction of the material was worked out based on the density of the GDL and then porosities were determined as 84±1% and 81±1% for carbon paper and carbon cloth respectively. Therefore those threshold values which give porosities out of 84±1% and 81±1% can be withdrawn. The average fibre diameter of the remaining threshold levels from the nanotomography images are given in Table (1a) and (1b).

The tomography threshold cannot be tuned with regard to porosity only. In our experiments, there are several values of porosities close to the reference values of 84±1% & 81±1% summarised in table (1a) and (1b). Each of the calculations represents different threshold levels.

In table (1a), number 2 can easily be removed because the calculated fibre diameter is higher than the others. Between 1, 3 and 4 the priority of choosing the optimal threshold is given to the fibre diameter since the experiment of fibre diameter average measurement was based on high resolution SEM images and therefore it is more accurate than density experiment. This leaves number 4 as the optimal threshold.

In table (1b), number 3 has the closest value of fibre diameter to the reference value, therefore this has been chosen as the optimal threshold for the GDL carbon cloth sample.

The fine-tuning process established above based on the conservation of fibre diameter and porosity therefore results in 84.9% and 81.8% of porosity and 7.1 μm and 8.7 μm in average fibre diameter for carbon paper and carbon cloth respectively. The 3D binary image of carbon paper and carbon cloth using optimal threshold values are shown in Figs. (4a) and (4b). The next step is to calculate the structural and fluid transport parameters of the representative Xray nanotomography-based 3D binary images.

STRUCTURAL PARAMETERS

Pore size distribution is a key characteristic of GDL structures [22]. A normal pore size distribution has been found based on Xray nanotomography result for both GDLs. Fig. (5a) shows that 12% of the pores are less than 7 μm in diameter (micropores and mesopores), 83% are between 7 μm and 20 μm (macropores) and finally 5% are more than 20 μm in the carbon paper. Corresponding values for the carbon woven cloth are 10%, 85% and 5% (Fig. 5b). The mean pore diameters are calculated as 15 and 11 μm for the carbon paper and carbon woven cloth respectively. Bernardi and Verbrugge [23] suggest that the pores that are less than 1 μm in diameter in the GDL can maintain a liquid phase pressure which is approximately 1 atm greater than the vapour phase pressure. Consequently, macropores (83%,85%) are capable of reducing mass transport limitations due to water flooding since they can provide diffusion paths for the catalyst layer while the smaller pores are closed-off by liquid water. The literature also suggests that pores with a diameter greater than 30 μm can hasten the onset of flooding [24]. In addition, the substantial presence of large pores can also compromise the electrical conductivity of the electrode. Overall it is desirable to limit the presence of pores above 30 μm in diameter to the overall pore size distribution of the GDL.

CALCULATION OF FLUID TRANSPORT PARAMETER

Permeability is a material property that describes the ease of the flow within the pore space of a medium. It is of great importance for determining the flow characteristics of the GDLs. LB model was employed to calculate the permeability. With the LB method it is relatively facile to deal with complicated boundaries and various forces at microscopic scales and overall therefore it becomes more efficient to simulate complex flows in porous media at pore scale.

The LB method is a numerical model developed over the past two decades to simulate fluid dynamics based on kinetic theory [25,26]. The concept of the LB method was to overcome some drawbacks of its predecessor, the lattice gas algorithm [27]. It was later found that the LB model can be derived directly from the continuous Boltzmann equation in kinetic theory [28].

The LB model operates by tracking the streaming and collision of a number of fictitious particles in a lattice in terms of particle distribution functions. The particle distribution function $f_i(x,t)$ defines the mass of a particle at location x at time t and moving with velocity I in the direction i:

$$\frac{\partial f_i(x,t)}{\partial t} + I \cdot \nabla f_i(x,t) = \frac{1}{\lambda}\left[f_i^{eq}(x,t) - f_i(x,t)\right] \tag{1}$$

where $f_i^{eq}(x,t)$ is the equilibrium distribution function which is the value of $f_i(x,t)$ under an equilibrium state and λ is a relational parameter which controls the rate at which $f_i(x,t)$ approaches $f_i^{eq}(x,t)$.

The LB model considers the particle distribution functions at each voxel in turn and determines a set of nineteen velocities in the 3D spatial domain for the node of each voxel. The nineteen velocities considered are as follow: stagnation at the origin $(0,0,0)/\partial t$; two velocities in the x direction $(\pm\partial x, 0,0)/\partial t$; two in the y direction $(0, \pm\partial x, 0)/\partial t$; four in the x-y plane $(\pm\partial x, \pm\partial x, 0)/\partial t$; four in the y-z plane $(\pm\partial x, 0, \pm\partial x)/\partial t$ and four in the y-z plane $(0, \pm\partial x, \pm\partial x)/\partial t$. This scheme is commonly known as the D3Q19 scheme. The singlephase model assumes that the pores of the GDL are infiltrated by air. Using the detailed velocity field, it is possible to calculate the three components of the permeability tensor for the imaged sample using Darcys law;

$$k_{xx} = \frac{\mu\rho q_x}{(\Delta P/L_x)}; \ k_{xy} = \frac{\mu\rho q_y}{(\Delta P/L_x)}; \ k_{xz} = \frac{\mu\rho z}{(\Delta P/L_x)} \tag{2a,b,c}$$

where ρ is the density of air, μ is the kinetic viscosity of air, q_i is the average velocity in the direction i, ΔP is the pressure applied in the principal flow direction and L_i is the overall sample length in the direction i. The average velocity qi is directly related to the velocity field and are obtained by:

$$q_x = \frac{\sum_i u_x(x_i)}{L_x L_y L_z}; \ q_y = \frac{\sum_i u_y(x_i)}{L_x L_y L_z}; \ q_z = \frac{\sum_i u_z(x_i)}{L_x L_y L_z} \tag{3a,b,c}$$

where $u_x(x_i)$, $u_y(x_i)$, $u_z(x_i)$ are the three simulated velocity components for each element of the image. Once the absolute permeability is known, the permeability for each specific gas with density ρ_j

and kinetic viscosity μ_j can be calculated from $K_j = k/\rho_j\mu_j$. All the variables in equations. $2 - 3$ are measured in a spatial unit δx and a temporal unit δt. Applying the pressure difference to other two directions allows the other components of the permeability tensor to be calculated.

In the LB model, a pressure difference is applied to two opposite sides of the image along the through-plane direction to drive gas flow. The other four sides at in-plane directions are treated as non-mirrored periodic boundaries, in which two opposite sides are neighboured such that particles moving out of the domain from one side re-enter the domain through its opposite side. All the simulations start from a zero velocity field and the pressure field is linearly distributed in the direction along which the pressure difference is imposed. Steady state conditions are adjudged using the parameter Ω where

$$\Omega = \frac{\sum_i |u_j(x_i, t+100) - u_j(x_i, t)|}{\sum_i u_j(x_i, t)}; \ (j = x, y, z) \tag{4}$$

Flow is assumed to have reached steady state when the tolerance $\Omega < 10^{-5}$ is satisfied.

In the current study, the both GDLs have porosities of greater than 80% which thereby eases the computational demand of the LB flow simulation. This therefore allows each voxel of the 3D binary image to be used directly as the lattices of the LB model. In this case, the spatial resolution of the LB model is set equal to the resolution of the X-ray images in the current work.

The LB solver is applied to the fine tuned samples of $100 \times 300 \times 100$ μm (300 μm corresponds to flow direction) to simulate the detailed gas velocity field in the void space of the GDL, with the assumption that the void space is infiltrated by air. The simulated velocity is then used to obtain the absolute permeability for the sample. Because the absolute permeability represents the linear dependence of gas flow rate on pressure gradient, it must be ensured that the flow rate in the simulations is also in this linear range. As such, the pressure difference applied to each sample is set to 20 Pa. The simulation is carried out on a dual-core 2.01 GHz workstation with 3.25 GB of RAM. A single-phase simulation for the region takes 500 minutes. The through plane and in-plane permeabilities $\left(k_{xx}, k_{xy}, k_{xz}\right)$ have been found as 4.02×10^{-7} mm^2, 5.07×10^{-8} mm^2 and 5.25×10^{-8} mm^2 respectively. Corresponding permeabilities for the GDL carbon cloth were obtained as 8.11×10^{-7} mm^2, 7.13×10^{-8} mm^2 and 7.64×10^{-8} mm^2.

Our previous work [29] reports a successful study into the combined full morphological reconstruction of fuel cell structures using X-ray computed microtomography and LB modelling to simulate fluid flow at pore scale in a GDL. The validation work demonstrates that the difference between the simulated and measured absolute permeability of air was 3%.

DISCUSSION AND CONCLUSIONS

In the digital model reconstruction of a porous material from Xray nanotomography scans, a small variation in threshold may have significant influence on fibre diameter and porosity. The current study establishes a method by which the threshold of X-ray nanotomography images can be fine-tuned based on high resolution SEM images and porosity measurements for the first time. The technique established by the current study provides a useful tool to determine the most precise threshold level for a variety of tomography techniques.

In experiments, it is found that a variation of more than 5% in threshold makes a significant visual difference to the resultant binary images, while a variation of less than 5% is difficult to be recognised visually, especially when there is no reference for comparison but can have a significant effect on the overall structural properties of 3D binary image. It is showed that the porosity increases linearly with the increase of threshold level. The linearity means that the structure is homogeneous in terms of material density distribution. The variation in threshold results in 10% fluctuation in the fibre diameter of the nanotomography image of the carbon paper. This could be because the fibres which are packed very closely together could be separated by only a slight variation in threshold, which can change the average diameter accordingly. After fine tuning of the threshold, 3D images were used to calculate key structural parameters and permeabilities of the porous media. The GDL samples used in the current work are found to have through-plane permeabilities of 4.02×10^{-7} mm^2 and 8.11×10^{-7} mm^2.

It has been proven that when a study is carried out using X-ray nanotomography data for porous materials such as a fuel cell GDL, the key structural parameters are affected by small variation in threshold. Having some easily measurable references such as porosity and average fibre diameter will greatly assist to finely tuning the threshold for the 3D binary representative image.

ACKNOWLEDGMENT

REFERENCES

[1] Haddad, W.S.; McNulty, I.; Trebes, J.E.; Anderson, E.H.; Levesque, R.A.; Yang, L. Ultrahigh-Resolution X-ray Tomography. Science, 1994, 266, 1213-1215.

[2] McNulty, I. Current and ultimate limitations of scanning x-ray nanotomography, Proc. SPIE , X-Ray Micro- and Nano-Focusing: Applications and Techniques II, I. 2001, 4499, 23-28.

[3] Zschech, E.; Yun, W.; Schneider, G. High-resolution X-ray imaging a powerful nondestructive technique for applications in semiconductor industry. Appl. Phys. A-Mater. 2008, 92, 423–429.

[4] McNulty, I.; Haddad, W.S.; Trebes, J.E.; Anderson, E.H. Soft X-ray Scanning Microtomography with Submicron Resolution, Rev. Sci. Instrum. 1995, 66 (2), 1431-1435.

[5] Sasov, A. X-ray nanotomography, developments in X-ray tomography IV. Proceedings of the SPIE, 2004, 5535, 201–211.

[6] Sinha, P.K.; Halleck, P.; Wang, C.Y. Quantification of Liquid Water Saturation in a PEM Fuel Cell Diffusion Medium Using X-ray Microtomography, Electrochem. Solid St., 2006, 9(7), A344-A348.

[7] Becker, J.; Schulz, V.; Wiegmann, A. Numerical determination of two-phase material parameters of a gas diffusion layer using tomography images. J. Fuel. Cell. Sci. Tech., 2008, 5(2), 021006-1-9.

[8] Barbir, F. PEM Fuel Cell: Theory and Practice. Elsevier Academic Press: London, 2005.

[9] Sinha, P.K.; Wang, C.Y. Pore-network modelling of liquid water transport in gas diffusion layer of polymer electrolyte fuel cell, Electrochim. Acta. 2007, 58(28), 7936-7945.

[10] Sinha, P.K.; Mukherejee, P.P.; Wang, C.Y. Impact of GDL structure and wettability on water management in polymer electrolyte fuel cells, J. Mater. Chem. 2007, 17(30), 3089-3103.

[11] Manke, I.; Hartnig, C.; Grunerbel, M.; Lehnert, W.; Kardjilov, N.; Haibel, A.; Hilger A.; Banahrt, J. Investigation of water evolution and transport in fuel cells with high resolution synchrotron x-ray radiography, Appl. Phys. Lett. 2007, 90(17), 174501-174505.

[12] Feser, J.P.; Prasad A.K.; Advani, S.G. Experimental characterization of inplane permeability of gas diffusion layers, J. Power Sources. 2006, 162(2), 1226-1231.

[13] Hung, T.F.; Huang, J.; Chuang, H.J.; Bai, S.H.; Lai Y.J.;Yang Y.W.C. Highly efficient single-layer gas diffusion layers for the proton exchange membrane fuel cell. J. Power Sources. 2008, 184(1), 165-171.

[14] Ostadi, H.; Jiang, K.; Prewett, P.D. Micro/nano X-ray tomography reconstruction fine tuning using scanning electron microscope images, Micro Nano Lett. 2008, 3(4), 106-109.

[15] Hara, T.; Tanck, E.; Homminga, J.; Huiskes, R.; The Influence of Micro Computed Tomography Threshold Variation on the Assessment of Structural and Mechanical Trabecular Bone Properties. Bone. 2002,23(2), 163-169.

[16] Ding, M.; Odgaard, A.; Hvid, I. Accuracy of cancellous bone volume Fraction measured by micro-CT scanning. J. Biomech. 1999, 32: 323-326.

[17] Bals, S.; Batenburg, K.S; Verbeeck, J.; Sijbers, J.; Van Tendeloo, G. Quantitative Three-Dimensional Reconstruction of Catalyst Particles for Bamboolike Carbon Nanotubes. Nano Letters, 2007, 7(12), 3669-3674.

[18] Zhang, X.; Crawford, J.W.; Bengough, A.G. Young IM. On boundary conditions in the lattice Boltzmann model for advection and anisotropic dispersion equation. Adv. Water Resour. 2002, 25, 601-609.

[19] Zhang, X.; Ren, L. Lattice Boltzmann model for agrochemical transport in soils. J. Contam. Hydrol. 2003, 67, 27-42.

[20] Wang, J.; Zhang, X.; Bengough A.G.; Crawford J.W. Domain-decomposition method for parallel lattice Boltzmann simulation of incompressible flow. Phys. Rev. E. 2005, 72, 016706 (1-11).

[21] Skyscan Microtomography. CT-Analyser Users Guide,Version 1.6.1, 2007.

[22] Kong, S.; Kim, D.Y.; Lee, H.K.; Shul, Y.G.; Lee, T.H. Influence of pore-size distribution of diffusion layer on mass-transport problems of proton exchange membrane fuel cells. J. Power Sources. 2002, 108, 185–191.

[23] Bernardi, D.M.; Verbrugge, M.W. A mathematical model of the solidpolymer- electrolyte fuel cell. J. electrochem. Soc. 1992, 139, 2477-2491.

[24] Wilson, M.S.; Valerio, J.A.; Gottesfeld, S. Low platinum loading electrodes for polymer electrolyte fuel cells fabricated using thermoplastic ionomers. Electrochim. Acta. 1995, 40, 355-363.

[25] Chen, H.; Chen, S.; Matthaeus, W.H. Recovery of the Navier-Stokes equations using a lattice-gas Boltzmann method. Phys. Rev. A. 1992, 45, R533- R5342.

[26] McNamara, G.R.; Zanetti, G. Use of the Boltzmann Equation to Simulate Lattice-Gas Automata. Phys. Rev. Lett. 1988, 61(20), 2332-2335.

[27] Frisch, U.; Hasslacher, B.; Pomeau, Y. Lattice-gas automata for the Navier – Stokes equation. Phys. Rev. Lett. 56, 1986,1505–1508.

[28] He, X.; Luo, L. A priori derivation of the lattice Boltzmann equation. Phys. Rev. E, 1997, 55, 6333-6336.

[29] Rama, P.; Liu, Y.; Chen, R.; Ostadi, H.; Jiang, K.; Zhang, X.; Fisher, R.; Jeschke, M. An X-ray tomography based Lattice Boltzmann simulation study on gas diffussion layers of polymer electrolyte fuel cells. J. Fuel. Cell. Sci. Tech. 2010, 7(1), 1-10.
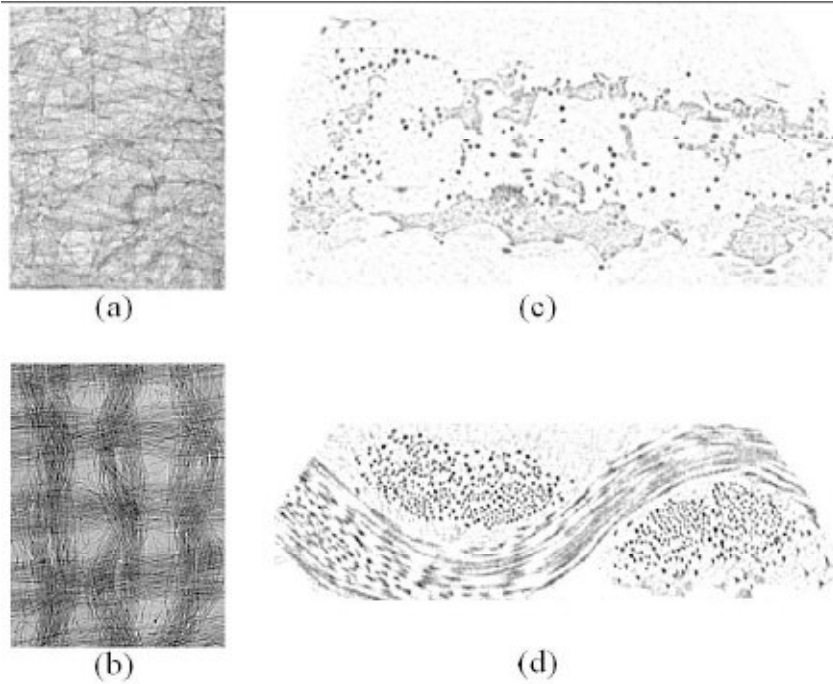
Fig. (1). X-ray tomographic images of GDL samples; (a) Shadow x-ray tomographic image of carbon paper sample; (b) Shadow x-ray tomographic image of carbon cloth sample; (c) A reconstructed 2D slice image of the carbon paper using CTAN software; (d) A reconstructed 2D slice image of the carbon cloth using CTAN software.
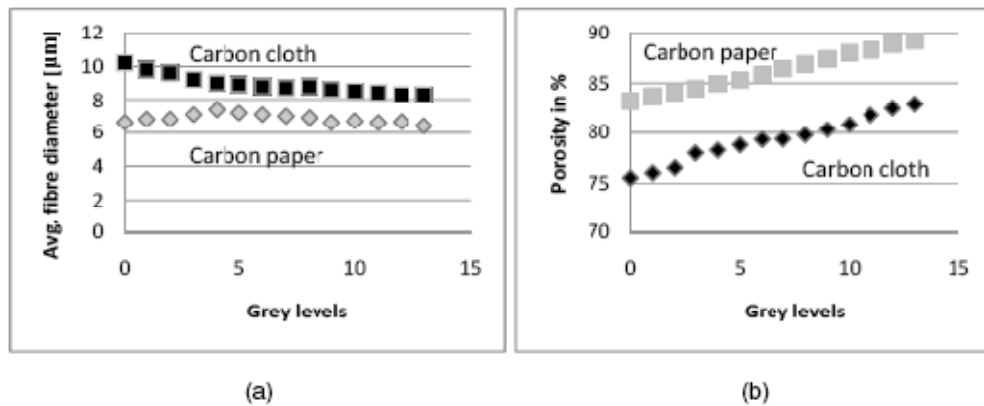

Fig. (2). Variation of fibre diameter and porosity over 5% threshold alteration. 13 grey levels represent 5% of threshold variation; (a) Average fibre diameter over threshold is fluctuating for GDL carbon paper and decreasing for carbon cloth; (b) Porosity changes linearly over threshold.
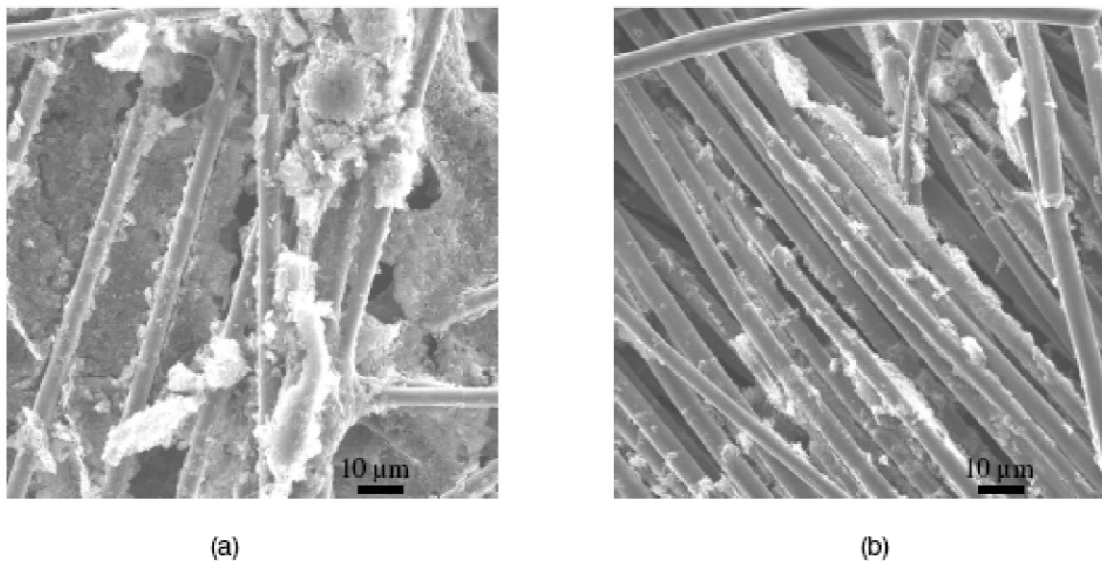
(a)   (b)

Fig. (3). SEM images of the surface of the GDL samples. The edges of the fibres are sharp and this greatly assisted to measure the diameter of fibres. (a) GDL carbon cloth; (b) GDL carbon paper.
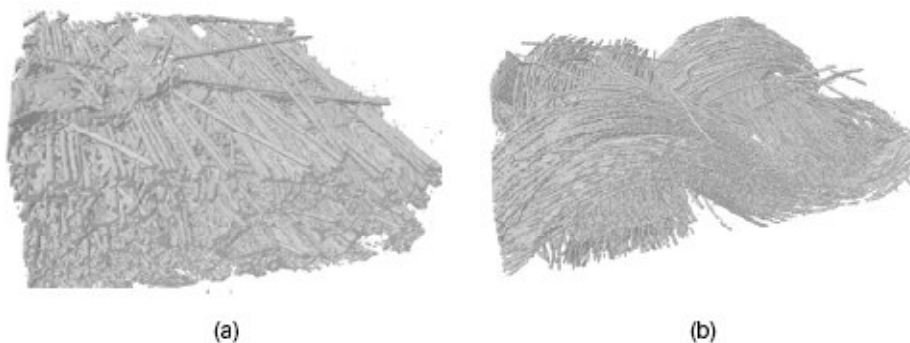

(a)   (b)

Fig. (4). 3D images of GDL samples; (a) An isometric view of the reconstructed image of GDL carbon paper sample with 680 nm resolution using CTAN; (b) An isometric view of the reconstructed image of GDL carbon cloth sample with 970 nm resolution using CTAN.
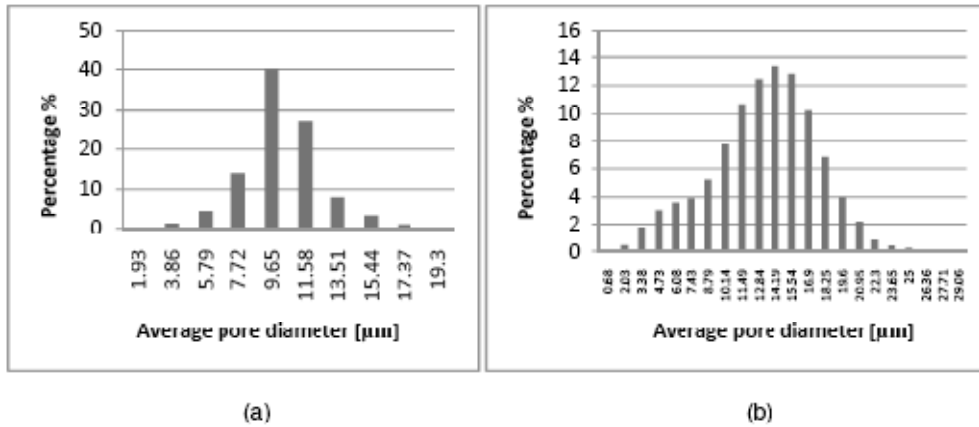
Fig. (5). 3D Pore diameter size distribution of GDL samples; (a) Carbon cloth, the mean pore diameter was found to be 11 µm; (b) Carbon paper, the mean pore diameter was found to be 15 µm.

Table 1a. Average Fibre Diameter of the Remaining Threshold Values, Reference Value of Fibre Diameter, Porosity Results from Nanotomography and Reference Value of Porosity for the GDL Carbon Paper

Number	Average Fibre Diameter (µm)	Reference Value of Fibre Diameter (µm)	Porosity (%)	Reference Value of Porosity
1	7.2	7.00±0.05	83.0%	84±1%
2	7.4	7.00±0.05	83.3%	84±1%
3	7.2	7.00±0.05	84.4%	84±1%
4	7.1	7.00±0.05	84.9%	84±1%

Table 1b. Average Fibre Diameter of the Remaining Threshold Values, Reference Value of Fibre Diameter, Porosity Results from Nanotomography and Reference Value of Porosity for the GDL Carbon Cloth

Number	Average Fibre Diameter (µm)	Reference Value of Fibre Diameter (µm)	Porosity (%)	Reference value of Porosity
1	8.9	8.40±0.05	80.3%	81±1%
2	8.8	8.40±0.05	80.8%	81±1%
3	8.7	8.40±0.05	81.8%	81±1%